Paleobiology, 43(3), 2017, pp. 407–424
DOI: 10.1017/pab.2016.57

PALEOBIOLOGY
A PUBLICATION OF THE Paleontological SOCIETY

Sexual shape dimorphism and selection pressure on males in fossil ostracodes

Tatsuhiko Yamaguchi, Rie Honda, Hiroki Matsui, and Hiroshi Nishi

Abstract.—Sexual dimorphism is thought to have evolved via selection on both sexes. Ostracodes display sexual shape dimorphism in adult valves; however, no previous studies have addressed temporal changes on evolutionary timescales or examined the relationships between sexual shape dimorphism and selection pressure and between sexual shape dimorphism and juvenile shape. Temporal changes in sexually dimorphic traits result from responses of these traits to selection pressure. Using the Gaussian mixture model for the height/length ratio, a valve-shape parameter, we identified sexual differences in the valve shape of *Krithe dolichodeira* s.l. from deep-sea sediments of the Paleocene (62.6–57.6 Ma) and estimated the proportion of females in the fossil populations at 11 time intervals. Because the proportion of females in a population is altered by the mortality rate of adult males, it is reflective of selection pressure on males. We attempted to correlate the height/length ratios between the sexes with the proportion of females, taking into consideration that the valve shape was not linked with the selection pressure on males. In time-series data of the height/length ratio, both sexes indicate no significant changes on evolutionary timescales, even though the sex ratio of the population changed from female skewed to male skewed during the late Paleocene. The sexual shape dimorphism was not driven by sexual selection. The static allometry between the height/length ratio and length indicates that the sexual shape dimorphism did not function for sexual display. The absence of change over time in the female allometric slope suggests that the evolution of valve shape was constrained by stasis.

Tatsuhiko Yamaguchi. Center for Advanced Marine Core Research, Kochi University, Monobe B200, Nankoku, Kochi, 783-8502, Japan. E-mail: tyamaguchi@kochi-u.ac.jp

Rie Honda. Department of Applied Science, Kochi University, 2-5-1 Akebono-cho, Kochi, Kochi, 780-8520, Japan

Hiroki Matsui. Department of Earth Science, Tohoku University, Aramaki Aza Aoba 6-3, Aoba-ku, Sendai, 980-8578, Japan

Hiroshi Nishi. Tohoku University Museum, Tohoku University, Aramaki Aza Aoba 6-3, Aoba-ku, Sendai, 980-8578, Japan

Accepted: 2 December 2016
Published online: 22 May 2017
Data available from the Dryad Digital Repository: http://doi.org/10.5061/dryad.14j2m.3

Introduction

Sexual dimorphism in fossils has the potential to explain the evolution of sex and sexual selection throughout geological time (Knell et al. 2013). Information from fossils is very important for understanding this aspect of evolution, because sexual selection works on evolutionary timescales (more than 1 million generations; Lande 1980). However, sexual dimorphism in fossils is not easily recognized (Knell et al. 2013; Motani et al. 2015). With the exceptions of very well preserved specimens (e.g., Matzke-Karasz et al. 2009; Siveter et al. 2014), most fossil specimens lack evidence for many types of sexual traits, such as the soft tissues of copulatory organs. In addition, they do not show direct evidence of sexual behaviors such as mating and breeding. Therefore, it is difficult to interpret the functions of traits in fossil specimens as sexual behavior. Identification of sexes is often difficult; in particular, an extinct taxon with extreme sexual dimorphism may often be misinterpreted as a completely different different taxon. For rare taxa such as megafossils, it is also difficult to collect sufficient specimens to obtain a statistically sufficient sample size (Padian and Horner 2013). Therefore, the evolution of sex and sexual dimorphism has seldom been investigated using fossils (Knell et al. 2013).

Fossil ostracodes show sexual dimorphism in the shape and size of their adult valves (e.g., Horne et al. 2002; Ozawa 2013). Many taxa show obvious sexual dimorphism in adult valves, and some taxa display sexual dimorphism even in juvenile valves (e.g., Kamiya 1988; Forel et al. 2015). Males generally have a more

 0094-8373/17

elongated valve shape than females. The allometry between valve length and height allows the assessment of the valve shape and the identification of the sex of living and fossil specimens (e.g., Ozawa 2013). Females have valves with higher height/length ratios than males. This ratio is a critical element in determining allometry: the static allometric slope and intercept are different between the sexes (e.g., Ikeya and Ueda 1988). Via ontogenesis, ostracodes grow by molting six to eight times in their life. Their valve shape changes with increasing valve size (Baltanás et al. 2000; Danielopol et al. 2008). After the final molt, they become adults, rapidly develop sexual dimorphism in their valves, and change their allometry between the valve length and height.

Sexual dimorphism may result in sexual selection. Sexual dimorphism in ostracode valve shape is correlated with either mating activity (swimming activity, mating position, or copulatory organ accommodation) and/or brooding (Cohen and Morin 1990). Abe (1990), who reviewed sex ratios in ostracode populations, concluded that sexual dimorphism is enhanced by selection pressures on both females and males. Previous studies have proposed that the sexual dimorphism in valves may have been affected by selection pressures on both sexes. An alternative hypothesis for the static allometry suggests that valve shape may be stable on evolutionary timescales. In the allometry law, the relationship between the valve length (L) and the valve height (H) is expressed as follows: $H = aL^b$, where the constants a and b are the allometric intercept and slope, respectively. Following the formula conversion of Bondurianskey and Day (2003), the valve shape (i.e., the H/L ratio) can be determined from the relation $H/L = aL^{b-1}$. Because it is hypothesized that the static allometric slope b has low evolvability (e.g., Egset et al. 2012; Firmat et al. 2014; Pélabon et al. 2014; Voje et al. 2014), H/L ratios have been stable on evolutionary timescales. The stability of the static allometric intercept a on million-year timescales is still a matter of debate (Voje et al. 2014). In general, sexual dimorphism is thought to have evolved in response to selection pressures that differ between males and females (e.g., Badyaev and Martin 2000). Sexual dimorphism is also affected by a combination of sexually dimorphic growth patterns and selection on individuals during growth (e.g., Badyaev et al. 2001). However, no previous studies have tested whether sexual differences in ostracode valves are correlated with selection pressure or have addressed the relationship between sexual shape dimorphism and juvenile shapes.

Sexual shape dimorphism is a phenotypic trait that responds to environmental changes. Temporal changes in phenotypic traits are very important for understanding selection and trait responses to selection, because the overall magnitudes and directions of adaptive evolution result in selection on these traits (Siepielski et al. 2009). If sexual shape dimorphism is affected by selection pressures on evolutionary timescales, time-series data of shape traits will show temporal changes and indicate characteristic patterns. Only a few studies have portrayed temporal changes in ostracode valve shape on million-year timescales (Reyment 1963, 1985; Hunt 2007a, 2013). Using the fossil record, temporal changes in phenotypic traits and their patterns can be determined on evolutionary timescales (e.g., Hunt et al. 2008; Firmat et al. 2014; Saito-Kato et al. 2015). In ostracode populations, the adult sex ratios (ASRs) indicate selection pressure on males. ASRs are reflective of male mortality rates (Kamiya 1988; Abe 1990; Rossi et al. 2004, 2013; Martins et al. 2009; Rossi and Menozzi 2012). In the populations of previous studies, the sex ratios are female biased, that is, more females survive than males after the final molting. If the sexual shape dimorphism is enhanced by selection pressure on males, the valve-shape parameter can be correlated with the ASR. Temporal changes in traits result from responses to selection pressure during growth. If the sexual dimorphism traits were affected by selection pressures on growing individuals, the temporal changes in the traits of each sex could be correlated with changes in the juvenile traits.

The aims of this study are: (1) to investigate whether ostracode valve shape exhibits temporal changes on million-year timescales; (2) to test whether valve shape is correlated with female ratios, which are an indicator of selection pressure on males; (3) to examine whether adult shape is correlated with juvenile shape; and (4) to analyze temporal changes in static allometry between the

https://doi.org/10.1017/pab.2016.57 Published online by Cambridge University Press

valve shape and the valve length. For this study, we used *Krithe dolichodeira* s.l. from Paleocene sediments at the Integrated Ocean Drilling Program Site U1407 off Newfoundland in the northwestern Atlantic. This species shows clear sexual dimorphism (Coles et al. 1994; Ayress et al. 1999) and is found in Cenozoic deep-sea sediments in the North Atlantic (Coles et al. 1994; Yamaguchi et al. 2017a,b). The sediments are continuous and well dated by means of planktic microfossil biostratigraphy (Norris et al. 2014; T. Yamaguchi, A. Bornemann, H. Matsui, and H. Nishi, unpublished observations). The ostracode specimens were obtained from successive discrete samples (Yamaguchi et al. 2017a,b).

Materials and Methods

Outline of the Methods.—Specimens of *Krithe dolichodeira* were collected from Paleocene sediment samples. We measured the valve length (L) and height (H) of the specimens and calculated the valve area, $\ln(L \times H)$. To examine the morphological variation of the specimens, we subjected a data set of $\ln(L \times H)$ to the Gaussian mixture model (GMM) and Bayesian information criterion (BIC) and grouped the specimens into morphotypes (for details, see the subsection on GMM and BIC below). For sexual identification, we calculated the H/L ratios of the specimens and applied the ratios in each morphotype to the GMM and BIC. Male populations show isolated clusters of H/L ratios compared with female populations (e.g., Ikeya and Ueda 1988; Ozawa 2013). In the genus *Krithe*, males show smaller H/L ratios than females (Athersuch et al. 1989; Coles et al. 1994; Ayress et al. 1999; Tanaka 2016). If the BIC indicates two groups in the H/L ratios of a morphotype, the morphotype likely has sexual shape dimorphism in the H/L ratio. Dividing the time range of the sediment samples, we set time intervals. In each time interval, we calculated the sex ratios and the mean, variance, and standard deviation of the H/L ratios in each sex using GMM. To capture the allometric relationship between L and the H/L ratios, we subjected the parameters in each time interval to simple linear regression and calculated the allometric slope and intercept. Using Hunt's (2006) method, which uses model fitting and selection, we examined the pattern of temporal changes in the H/L ratios of females and males and in the allometric slope and intercept.

Sediment Samples.—Yamaguchi et al. (2017a,b) studied the taxonomy of ostracodes from Upper Cretaceous and Paleocene sediments at the Integrated Ocean Drilling Program Site U1407 (41°25′30″N, 49°48′28.8″W: Norris et al. 2014). Three cores were drilled into the seafloor of the Southeast Newfoundland Ridge at a present-day water depth of 3073 m. The core diameter was ~6.8 cm. The Upper Cretaceous and Paleocene sediments are pinkish-to-white nannofossil chalks (Norris et al. 2014). Between the core composite depth below sea floor (CCSF) of 214 m and 205 m, the sediments are a greenish color. At ~205 m CCSF, the lithology of the sediments is divided into two subunits: nannofossil chalks with radiolarians above ~205 m CCSF and nannofossil chalks below ~205 m CCSF. The seafloor is estimated to have been at a depth of 1800 m at 60 Ma (Norris et al. 2014). For this study, we used *Krithe dolichodeira* s.l. from 80 samples in the interval between 146.10 m CCSF and 211.83 m CCSF (the Paleocene). Samples with volumes of 10–30 cm^2 were separated from the core sediments using fan-shaped plastic scoops. One scoop can seize a quarter-cylinder of sediment with an area of ~5 cm^2 and a thickness of 1–2 cm. To obtain a single sediment sample, one or two plastic scoops were used. We discuss the fossil populations in a sediment volume of approximately 5–10 cm^2.

Age Model of the Core Sediments.—The timescale used here follows the Geological Time Scale 2012 (Gradstein et al. 2012). The core sediments are dated as latest Cretaceous and Paleocene using calcareous nannofossil biostratigraphy and carbon stable isotopes of the bulk sediments (T. Yamaguchi, A. Bornemann, H. Matsui, and H. Nishi, unpublished observations). We determined the geological ages of the sediment samples in the interval of 146.10–211.83 m CCSF using five datum events of calcareous nannofossil biostratigraphy (Supplementary Table 1). The geological ages of the sediment samples range from 62.60 to 56.87 Ma (Supplementary Table 2).

Measurements.—We measured the L and H of 187 adult and 76 juvenile specimens of *Krithe dolichodeira* s.l. from 80 Paleocene samples (Supplementary Table 2). Adult specimens can

https://doi.org/10.1017/pab.2016.57 Published online by Cambridge University Press

be discriminated from juvenile specimens via the presence of a broad anterior marginal zone and multiple marginal pore canals (e.g., Coles et al. 1994; Horne et al. 2002; Fig. 1). For the measurements, we used a digital microscope, VHX-2000 (Keyence), at the Center for Advanced Marine Core Research at Kochi University (Supplementary Table 2). The measurements were carried out at a magnification of 300×. The precision (1σ) of the measurements was ±0.645 μm as estimated from 90 repeated measurements obtained using a Zeiss stage micrometer (length: 1 mm).

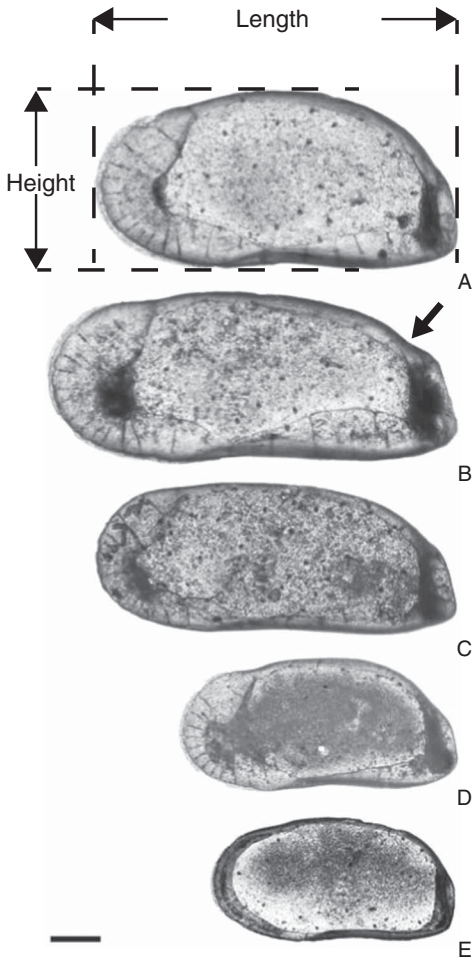

FIGURE 1. Light microscopy images of *Krithe dolichodeira* s.l. viewed inside the valves. Scale bar, 100 μm. A–E, *K. dolichodeira* s.l.: A, morphotype B, right valve, adult (342-U1407A-21X-4W, 74-76); B, morphotype B, right valve, adult (342-U1407A-21X-4W, 74-76); C, morphotype B, right valve, adult (342-U1407C-17X-6W, 110-112.5); D, morphotype S, right valve, adult (342-U1407C-14X-4W, 34-36.5); and E, right valve, juvenile (342-U1407C-16X-2W, 73-75). The measurements of the specimens are provided in Supplementary Table 2. An arrow indicates the truncation in the posterior margin.

GMM and BIC.—The GMM assumes that the measurements of individuals are normally distributed. Given a sample of measurements, the goals of the method are to choose the model with the number of groups that best fit the data and to provide a full distributional description, for example, the mean and variance for each subcomponent (Hand et al. 2001; Hunt and Chapman 2001). For model selection, BIC (Schwarz 1978) is widely used. In the example in Figure 2, the highest BIC indicates that the model with two subcomponents provides the best fit of the hypothetical candidate models. Using GMM clustering, Hunt and Chapman (2001) recognized clusters of eight growth stages in a trilobite population. We used GMM clustering to recognize the morphotypes and the sexual dimorphism. First, to recognize the number of morphotypes in *K. dolichodeira* we entered the data set of the valve area, $\ln(L \times H)$, into the GMM clustering. Next, to identify sex in each morphotype, we applied the same method to data sets of the H/L ratio in each morphotype.

In the GMM in this study, the general form of a mixture distribution for a value x, $\ln(L \times H)$, or the H/L ratio is defined as

$$f(x) = \sum_{k=1}^{K} w_k f_k(x \mid \Theta_k), \qquad (1)$$

where w_k is the mixing proportion or weight of the kth subcomponent, K is the number of subcomponents, $f_k(x)$ is the density distribution, and Θ_k is a set of parameters included in the distributional model. The mixing proportions (w_k) must lie between 0 and 1 and sum to 1.

The Gaussian distribution for a density distribution, $f_k(x)$ is defined as

$$f(x \mid \Theta_k) = \frac{1}{\sqrt{2\pi\sigma_k^2}} \exp\{-\frac{(x-\mu_k)^2}{2\sigma_k^2}\}, \qquad (2)$$

where σ_k^2 is the variance of the variable x, μ_k is the mean of the x values, and $\Theta_k = (\sigma_k^2, \mu_k)$. w_ks and Θ_k are determined using the expectation and maximization approach (Dempster et al. 1977). This approach enables the parameter set of w_k and Θ_k in the Gaussian density distribution to be calculated. The parameters

https://doi.org/10.1017/pab.2016.57 Published online by Cambridge University Press

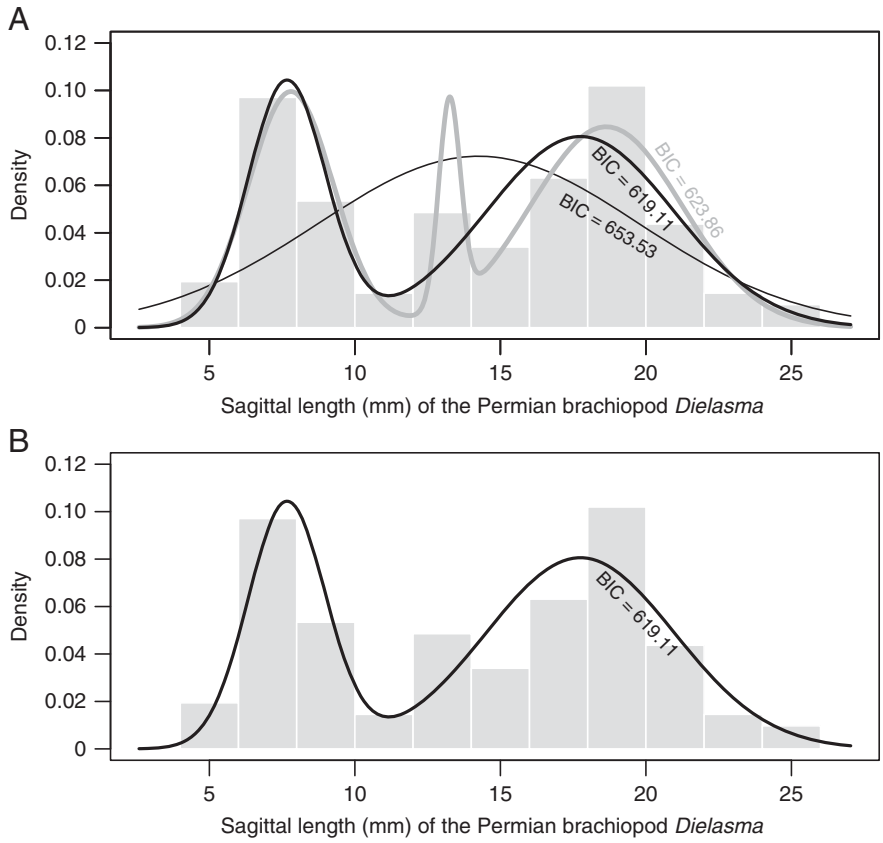

FIGURE 2. A, Histogram of the sagittal length of the Permian brachiopod *Dielasma*. The GMM generated density curves for the candidate models. The BIC score was calculated for each model. B, The density curve of the bimodal distribution was selected as the best-fit model because it had the lowest BIC score. The data were sourced from Hammer et al. (2001).

are determined to maximize the likelihood score function defined by

$$\Lambda = \sum_{i=1}^{n} \ln \left\{ \sum_{k=1}^{K} w_k f_k(x_i \mid \mu_k, \sigma_k^2) \right\}. \quad (3)$$

The parameter estimation consists of two steps, an E step and an M step. The initial values of the mean, μ_k, and the other parameters, w_k and σ_k^2, are given appropriately. In the E step, given an estimate of the subcomponent means, μ_k, variances, σ_k^2, and mixing proportions, w_k, the conditional probability that a data point x_i belongs to the jth subcomponent is calculated:

$$P_{ij} = \frac{w_j f_j(x_i \mid \mu_i, \sigma_i^2)}{\sum_{k=1}^{K} w_k f_k(x_i \mid \mu_k, \sigma_k^2)}. \quad (4)$$

In the M step, the parameters are estimated from the data, given the conditional probabilities P_{ij} (e.g., Celeux and Govaert 1995). The E and M steps are iterated until convergence, after which an observation can be assigned to the subcomponent or cluster corresponding to the highest conditional or posterior probability.

We used the BIC to subtract a term from the maximizing values of the likelihood. The formula for calculating the BIC is

$$\mathrm{BIC} = -2 \ln L(\theta) + d_k \ln N, \quad (5)$$

where, for a mixture model with K subcomponents, $\ln L(\theta)$ is the maximizing value of the positive log-likelihood and d_K is the number of free parameters to be estimated. N indicates the number of specimens. Both the number of subcomponents K, and the set $\{w_k, \mu_k, \sigma_k^2 \mid k = 1, 2, \ldots K\}$ with the lowest BIC value are selected as parts of the most optimized model. For this calculation, we used R software (R Core Team 2015) and its 'mclust' packages (Fraley et al. 2012).

https://doi.org/10.1017/pab.2016.57 Published online by Cambridge University Press

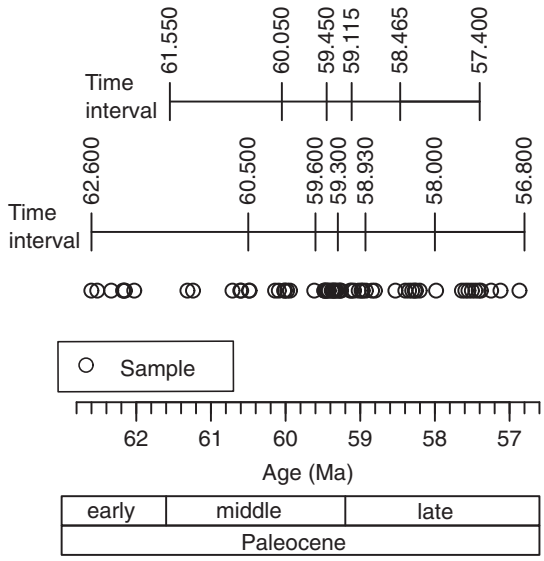

FIGURE 3. Time intervals and the temporal distribution of the sediment samples.

Sex Identification and Sex Ratio.—As mentioned earlier, males form an isolated cluster with respect to females in plots of L versus H (e.g., Ikeya and Ueda 1988; Horne et al. 2002; Ozawa 2013; Forel et al. 2015). In the *Krithe* species, males have smaller H/L ratios than females (Athersuch et al. 1989; Coles et al. 1994; Ayress et al. 1999; Tanaka 2016). When a taxon has an obvious sexual shape dimorphism, the optimal distribution of the H/L ratios is bimodal. The sex ratio is defined as the proportion of females to the total number of adult individuals. This is the ASR, which is also called the tertiary sex ratio. We consider each valve specimen to be an individual.

Time Intervals.—We divided the period of 62.6–56.8 Ma into 11 overlapping intervals (Fig. 3). First, we created six intervals: 58.93–56.8 Ma, 59.3–58.93 Ma, 59.6–59.3 Ma, 60.5–59.6 Ma, and 62.6–60.5 Ma. These intervals were designed to have 19–22 adult specimens. Next, linking the middle of one interval with that of the next interval, we created five additional intervals: 58.465–57.4 Ma, 58.465–58.115 Ma, 59.45–59.115 Ma, 60.05–59.45 Ma, and 61.55–60.05 Ma. The former six intervals overlap the latter five intervals. The durations of each interval range from 0.3 to 2.1 Myr. Each time interval has specimens of 10^5–10^6 generations, because ostracode longevity is several months to 1 yr (Cohen and Morin 1990). The variety in the duration of the intervals may affect the phenotypic variation (i.e., the variances of the H/L ratios) in the fossil record (Hunt 2004a). Hunt (2004a,b) demonstrated the relationship between the phenotypic variation of fossils and the durations of the samples containing the fossils; time averaging inflates the variation by less than approximately 5%. Therefore, the bias in phenotypic variation resulting from time averaging is sufficiently small and can be ignored.

Correlation Analysis.—Using Pearson's correlation and Student's t test, we examined the correlations between the proportion of females and the H/L ratios of both sexes and juveniles.

Allometry between L and the H/L Ratio.—Using a simple linear regression, we attempted to calculate the allometry equation between L and the H/L ratio in both sexes at each time interval:

$$\log_{10}\left(\frac{H}{L}\right) = \log_{10}(a) + b\log_{10}(L). \qquad (6)$$

When a significant correlation was recognized at the 0.05 level or less in the equation, the intercept, $\log_{10}(a)$, and the slope, b, were estimated.

Assessment of Temporal Changes in Traits.—Following the method of Hunt (2006), we tested the goodness of fit of the models for temporal changes in the H/L ratios and L of each sex and in the allometric slope and intercept. The method uses two assumptions: (1) genetic drift is not treated as a null model; and (2) adaptive evolution is equated with relentless directional selection. For the model fitting, we examined the five models defined by Hunt (2006, 2008) and Hunt et al. (2008, 2015): general random walk; unbiased random walk; stasis; strict stasis; and the Orstein–Uhlenbeck process. The general random walk model for directional evolution consists of a succession of random steps with a directional trend (Hunt 2006, 2008). The directional trend occurs when environmental or biotic factors that govern the position of phenotypic optimum peaks are stationary in the long term (Hansen 2012). The unbiased random walk for the random walk model lacks a directional trend. Stasis is an evolutionary

https://doi.org/10.1017/pab.2016.57 Published online by Cambridge University Press

trajectory with a constant mean; deviations around that mean are uncorrelated and normally distributed (Sheets and Mitchell 2001). A random walk can result from neutral genetic drift or from randomly varying natural selection (Hunt 2007b). The stasis mode is caused by genetic constraints or genetic drift among populations and by stabilized selection that fixes the adaptive peak or forces it to fluctuate around a steady mean (Hunt and Rabosky 2014). Strict stasis is the stasis with zero variance around the long-term mean. It represents no real change on evolutionary timescales (Hunt et al. 2015). The Orstein–Uhlenbeck process is natural selection with a combination of directional and stabilizing selection and is likely caused by the microevolution of a population in the vicinity of a fixed adaptive peak (Hunt et al. 2008). Calculating the bias-corrected Akaike information criterion and the Akaike weight in each model, the model with the highest Akaike weight value is selected as the best-fit model (e.g., Anderson et al. 2000). Hunt (2008) proposed two methods for model parameterization: ancestor–descendant and joint parameterizations. Ancestor–descendant parameterization uses the morphological differences between each ancestor–descendant pair of populations, whereas joint parameterization considers the joint distribution of traits across all sampled populations. Here, we selected joint parameterization, because we address the temporal changes in the traits of a single species. The parameters for the model fitting, means, variances, and numbers of individuals were obtained. Multiplying the number of individuals by the female or male ratio, we calculated the numbers of females and males, respectively. For the age of each time interval, we used the mean geological ages of the sediment samples with adult specimens. For the model fitting and selection, we used R's 'paleoTS' package (Hunt 2015).

Results

The Density Distribution of ln($L \times H$) and the Morphotypes.—The BIC scores indicate two subcomponents in valve area, ln($L \times H$) (Table 1): one group with an ln($L \times H$) of 12.34–12.96 and another group with an ln($L \times H$) of 12.06–12.30 (Fig. 4). The large and small groups consist of 126 and 61 specimens, respectively. The two groups are found from 62.6 to 56.87 Ma (Fig. 4A). Both groups share the outline, vestibulum shape, and the shape and number of marginal pore canals with *K. dolichodeira* (Fig. 1). The Coles et al. (1994) specimens of *K. dolichodeira* indicate an ln($L \times H$) of 12.03–12.76. Therefore, we treat the two groups as morphological variations of *K. dolichodeira* and call the large and the small groups morphotypes B and S, respectively.

TABLE 1. The Bayesian information criterion (BIC) scores and the number of subcomponents in the Gaussian mixture model for ln($L \times H$). The degree of freedom (d_K), the log-likelihood (lnΛ), and number of subcomponents (K) are given. Bold type indicates the lowest BIC value.

Number of subcomponents (K)	d_K	lnΛ	BIC
1	2	37.35	−64.23
2	5	61.18	**−96.20**
3	8	66.71	−91.57
4	11	71.49	−85.44
5	14	74.37	−75.51
6	17	74.53	−60.13
7	20	77.84	−51.06
8	23	77.83	−35.34
9	26	83.46	−30.90

The Density Distribution of the H/L Ratio.—The BIC scores indicate a bimodal distribution in morphotype B and a trimodal distribution in morphotype S (Fig. 5A,B, Table 2). Morphotype B likely appears due to sexual dimorphism in the adult valve shape, while morphotype S does not exhibit sexual dimorphism. Morphotypes B and S comprise 126 and 61 specimens, respectively. We chose to investigate morphotype B. Juveniles of the species are difficult to tell apart from juveniles of the *Krithe* sp. of Yamaguchi et al. (2017b). We measured juvenile specimens from samples that contained only adult morphotype B. In the juveniles, the BIC scores indicate a unimodal distribution (Fig. 5C, Table 2). The morphotype B data set constitutes measurements of a mixture of left and right valves. Right valves do not differ significantly from left valves in their mean H/L ratios (Supplementary Fig. 1). Welch's t-test failed to reject the null hypothesis that the means of the H/L ratios are equivalent between the left and right valves at a 0.05 significance level ($t = 1.5646$, df = 114.7, two-tailed $p = 0.12$). In the bimodal model of

https://doi.org/10.1017/pab.2016.57 Published online by Cambridge University Press

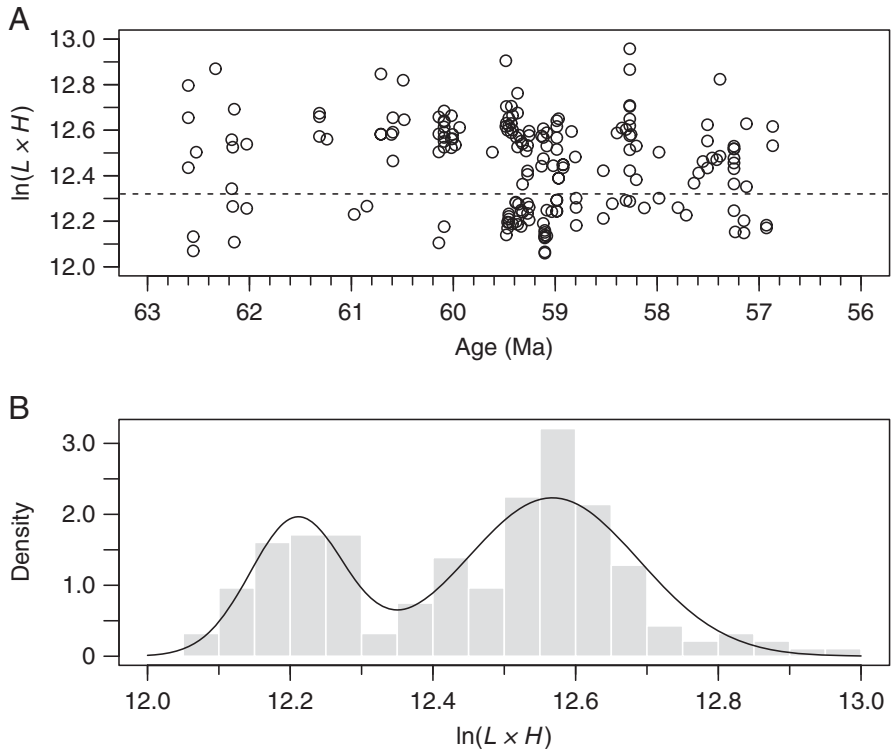

FIGURE 4. A, Plot of the age versus the area, ln ($L \times H$), of the valves. The dotted line indicates a ln($L \times H$) of 12.32. B, Histogram of ln($L \times H$) values in adult *Krithe dolichodeira*. The curve is the density estimation of the Gaussian mixture model with two subcomponents.

morphotype B, the means and standard deviations (1σ) are as follows: 0.423 ± 0.0142 and 0.492 ± 0.0164, with 51 and 75 specimens, respectively. We consider the groups with the smallest mean and with the largest mean to be the males and females, respectively. The identification of the sex is discussed in the next section. The GMM indicates a bimodal population for all the adults and a unimodal population for all the juveniles (Fig. 5C).

Correlation Analyses.—We calculated the proportion of females (i.e., the ASRs) and the means, variances, and standard deviations of the H/L ratios in each time interval. In the correlation between these calculated values, we recognized a significant correlation in the H/L ratios between the females and juveniles (Fig. 6, Table 3).

Allometry.—In six time intervals (58.0–56.8 Ma, 58.465–57.4 Ma, 58.93–58.0 Ma, 59.45–59.115 Ma, 59.6–59.3 Ma, and 60.05–59.45 Ma), the female H/L ratios correlate significantly with L (Fig. 7, Table 4). Conversely, the male H/L ratios have a significant correlation with L only in the interval of 59.115–58.465 Ma.

Time-Series Data of ASRs, H/L Ratios, and Allometric Slope and Intercept.—The ASRs range from 0.45 to 0.73 and decrease to less than 0.5 in the intervals of 58–56.8 and 59.30–58.93 Ma in the late Paleocene (Fig. 8A, Supplementary Table 3). The means of the female H/L ratios show a fluctuation between 0.484 and 0.499, while those of the male H/L ratios display a change from 0.417 to 0.428 (Fig. 8B, Supplementary Table 3). The juvenile H/L ratios exhibit means of 0.511–0.548. The female allometric slope and intercept change from −0.388 to −0.247 and from 0.406 to 0.812, respectively (Fig. 8C,D, Supplementary Table 4). In the interval of 59.115–58.465 Ma, we see a significant allometric relationship between the male L and H/L ratio (Table 4). The allometric slope and intercept are 0.58 and −2.06, respectively (Supplementary Table 4).

Temporal Changes in Valve-Shape Trait.—The output of the model fitting is summarized in Table 5. For the H/L ratios of both sexes, the strict

https://doi.org/10.1017/pab.2016.57 Published online by Cambridge University Press

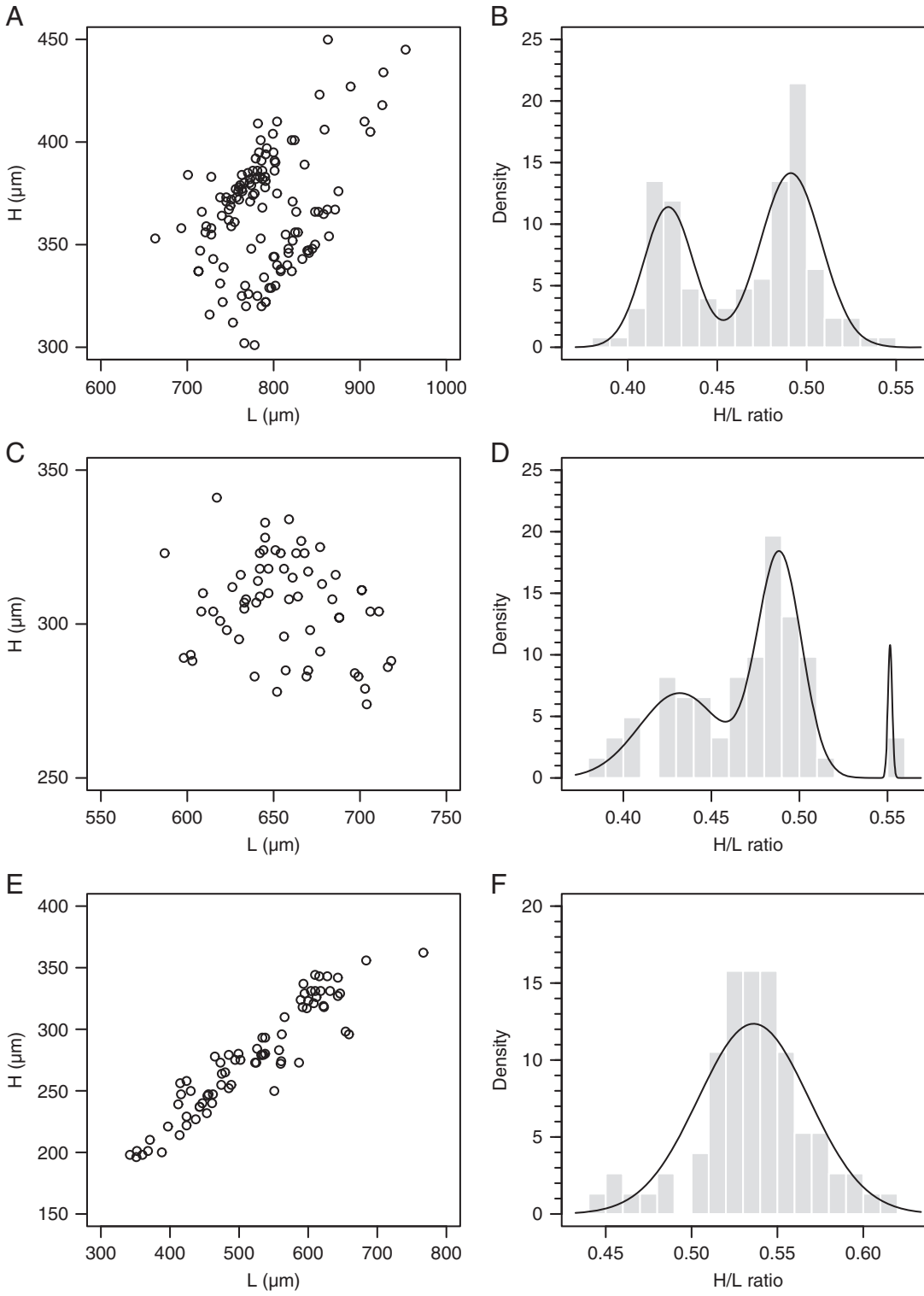

FIGURE 5. A, Plot of *L* and *H* in morphotype B. B, Histogram of the *H*/*L* ratios in morphotype B. The curve is the density estimation of the GMM with two components. C, Plot of *L* and *H* in morphotype S. D, Histogram of the H/L ratios in morphotype S. The curve is a density estimation of the GMM with three components. E, Plot of *L* and *H* in juveniles. F, The histogram of the *H*/*L* ratios in juveniles. The curve is the density estimation of the GMM with one component.

https://doi.org/10.1017/pab.2016.57 Published online by Cambridge University Press

TABLE 2. The Bayesian information criterion (BIC) scores and the number of subcomponents in the Gaussian mixture model for the H/L ratios. The degrees of freedom (d_K), the log-likelihood (lnΛ), and number of subcomponents (K) are given. Bold type indicates the lowest BIC value.

Number of subcomponents (K)	d_K	Morphotype B ($n = 126$)		Morphotype S ($n = 61$)		Juvenile ($n = 76$)	
		lnΛ	BIC	lnΛ	BIC	lnΛ	*BIC*
1	2	236.47	−463.27	116.42	−224.61	153.07	**−297.47**
2	5	265.63	**−507.08**	119.34	−218.12	156.97	−292.28
3	8	272.52	−506.34	129.41	**−225.93**	160.27	−285.89
4	11	272.94	−492.68	131.32	−217.43	162.89	−278.14
5	14	273.35	−478.98	129.03	−200.51	162.38	−264.14
6	17	273.91	−465.61	136.31	−202.73	162.4	−251.18
7	20	278.57	−460.41	136.75	−191.28	173.98	−261.35
8	23	281.78	−452.32	139.34	−184.14	174.26	−248.9
9	26	287.86	−449.97	139.63	−172.37	171.39	−230.17

stasis model is supported more strongly than the other models. The relative support for the Orstein–Uhlenbeck model is negligible. For the slope and intercept in the female allometry equations, the strict stasis model is also accepted as the best-supported model, accounting for 86% of the Akaike weight (Table 5). Therefore, the H/L ratios of both sexes and the allometric slope and intercept exhibit no real evolution between 61 and 57 Ma (Fig. 8B–D).

Discussion

Sexual Shape Dimorphism and Sex Identification.—In the anatomy of living *Krithe*, specimens with male copulatory organs are more elongate than specimens without the organ (Tanaka 2016). *Krithe dolichodeira* shows strong sexual dimorphism in adult valves (Coles et al. 1994). Males have slenderer valves than females. In the Coles et al. (1994) specimens, the mean and standard deviation (1σ) of the H/L ratios are 0.48 ± 0.024 in females and 0.43 ± 0.0053 in males. Coles et al. (1994) also noted that the male valves show more distinct truncation concavity in the posterior margin (Fig. 1B) than do the female valves. However, we recognized female specimens with distinct truncations in the specimens of Coles et al. (1994: Text-fig. 3I, N) and Ayress et al. (1999: Fig. 3G) and a male specimen without truncation in the specimens of Coles et al. (1994: Text-fig. 3Q). Therefore, we believe that the truncation is not a sexual dimorphic trait.

In the plot of L and H (Fig. 5A), the lack of clear coeval clusters may have been caused by the variable sizes of the species. In fossil ostracode populations that result from the accumulation of valves over a long time, instar and adult clusters cannot be straightforwardly recognized (Danielopol et al. 2008). Ostracodes changed their valve size and growth pattern over geological time (e.g., Hunt and Roy 2006; Hunt et al. 2010; Yamaguchi et al. 2012; Forel et al. 2015). A continuous distribution of L and H may have resulted in changes in the valve size during the Paleocene. As mentioned earlier, the BIC scores for the H/L ratios in morphotype B indicate two Gaussian subcomponents (Fig. 5B, Table 2). We interpret these two subcomponents as representing sexual dimorphism, not two species. Both subcomponents occur together in the samples, indicating that they dwelled contemporaneously in the same environment. All the specimens of both subcomponents possess the diagnostic characters of *Krithe dolichodeira* s.l. (Yamaguchi et al. 2017b), as indicated by the taxonomy of Coles et al. (1994). The juvenile population does not exhibit dimorphism (Fig. 5F, Table 2), suggesting that the dimorphism appeared in the adult stage. The difference in the H/L ratios between the subcomponents is consistent with sexual dimorphism in adult valves of morphotype B. Therefore, the adult dimorphism is thought to indicate the sexes. The subcomponent with the smallest mean is observed in males, and the subcomponent with the largest mean is observed in females.

Growth and Sexual Shape Dimorphism.—During growth from juvenile to adult, the valve shape becomes more elongated and the variation decreases. Both sexes show higher means of H/L ratios than do juveniles,

https://doi.org/10.1017/pab.2016.57 Published online by Cambridge University Press

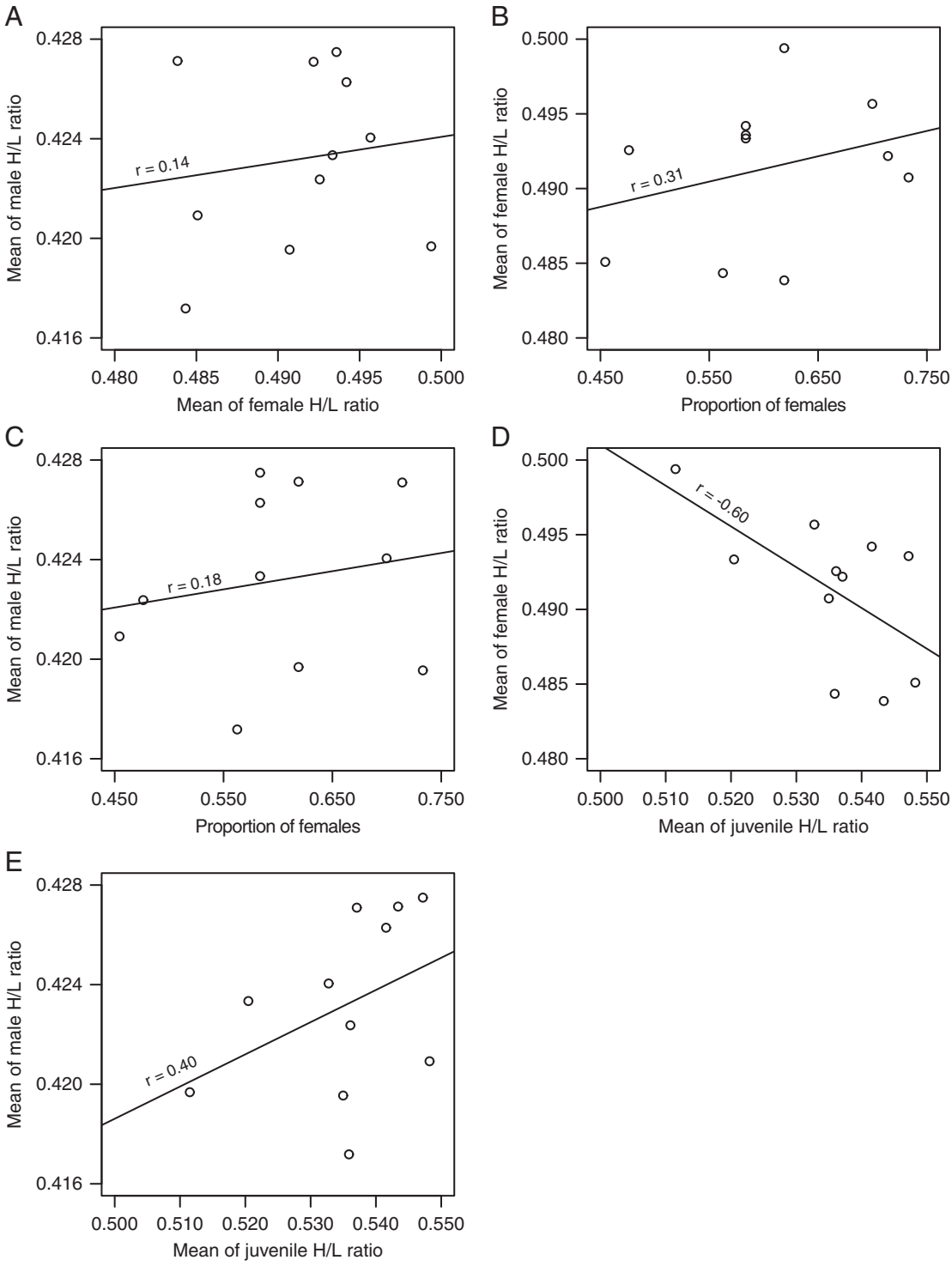

FIGURE 6. Plots of shape ratios. A, Mean of female H/L ratio versus male H/L ratio; B, proportion of females versus mean of female H/L ratio; C, proportion of females versus mean of male H/L ratio; D, mean of juvenile H/L ratio versus mean of female H/L ratio; and E, mean of juvenile H/L ratio versus mean of male H/L ratio. r is the correlation coefficient. For detailed statistical results, see Table 3.

https://doi.org/10.1017/pab.2016.57 Published online by Cambridge University Press

TABLE 3. Results of the linear regression analyses. The asterisk indicates significance at the 0.05 level; 95% CI and t_9 represent the 95% confidence interval and the *t*-value at nine degrees of freedom, respectively; R2 is the coefficient of determination.

Explanatory variable: X	Response variable: Y	Equation	95% CI	t_9	R^2	p
Mean of male H/L ratios	Mean of female H/L ratios	$Y = 1.0 \times 10^{-1}X + 3.7 \times 10^{-1}$	−0.50 to 0.68	0.43389	0.02	0.67
Proportion of females	Mean of female H/L ratios	$Y = 1.7 \times 10^{-2}X + 4.8 \times 10^{-1}$	−0.36 to 0.77	0.3611	0.093	0.36
Proportion of females	Mean of male H/L ratios	$Y = 7.3 \times 10^{-3}X + 4.2 \times 10^{-1}$	−0.47 to 0.71	0.5896	0.034	0.59
Mean of juvenile H/L ratios	Mean of female H/L ratios	$Y = -2.7 \times 10^{-1}X + 6.4 \times 10^{-1}$	−0.88 to −0.0061	0.04919	0.36	0.049*
Mean of juvenile H/L ratios	Mean of male H/L ratios	$Y = 1.3 \times 10^{-1}X + 3.5 \times 10^{-1}$	−0.26 to 0.81	0.2241	0.16	0.22

indicating slenderer valve shapes. The standard deviation of the adult H/L ratio is obviously smaller than that of the juveniles, except for the data in the time interval of 58.0–56.8 Ma; therefore, maturation alters both valve shape and size in *K. dolichodeira* s.l. as in the *Candona* species, *Cytherissa lacustris*, and *Eucypris virens* of Danielopol et al. (2008). The female H/L ratios have a significant correlation with the juvenile ratios (Fig. 6, Table 3), suggesting an effect of allometric constraints on the female shape. Conversely, the male H/L ratios do not have a significant correlation with the juvenile ratios. The effects of the allometric constraints differ between the sexes.

Ostracode ASR as Reflective of Selection Pressure on Males.—Under the assumption of the preservation of all dead valves, fossil ASRs indicate the productivity of both sexes in the long term (Abe 1990). Abe (1990) also assumed that (1) the valves would not be sorted by sexual shape dimorphism when dead valves are transported after the death of individuals; and (2) the predators for ostracodes would not favor one sex. A cohort with an even ASR would suffer from male-biased mortality. The living cohort would show a high ASR every month. The dead population, which is formed from the annual accumulation of dead specimens of the cohort, would exhibit an even ASR (Abe 1983, 1990). Under these assumptions, ASRs in dead populations would not show sex-biased mortality during seasons or in the short term, but would indicate the sex ratios at the maturation of the cohort. If the secondary sex ratios are even, skewed ASRs reflect sex-biased mortality just before maturation. The core sediments of the nannofossil ooze do not display stratigraphic changes in grain size (Norris et al. 2014), suggesting stable depositional environments without turbulence through the Paleocene. These stable environments allow us to assume that there was no transportation of dead valves. Székely et al. (2014) summarized four mutual factors that affect ASRs: (1) biased primary and secondary sex ratios; (2) sex-differential mortality; (3) different maturation rates in males and females; and (4) sex differences in dispersion pattern and habitats. In field observations of living populations, ostracode ASRs are not consistent with juvenile and offspring sex ratios. Abe (1990) summarized the proportion of females of seven brackish and marine taxa during the A − 1 and A stages. The A − 1 stage is the juvenile stage prior to the final molt, and the A stage is the adult stage. The ASRs are lower than the proportion of females in the A − 1 stage. Vandekerkhove et al. (2007) examined offspring sex ratios in cultivated *Eucypris virens* populations having different ASRs. They found that the female-biased population was derived from an even, sex-unbiased population. Kamiya (1988), Abe (1990), and Rossi et al. (2013) postulated that increases in the proportion of females from the A − 1 stage to the A stage result from increases in male mortality after the final molt. Different maturation rates between the sexes in ostracodes have been reported. In female-biased populations, field observations and culture experiments on living ostracodes suggest that ASRs are influenced by sexual differences in mortality and life span more strongly than are juvenile sex ratios (Kamiya 1988; Martins et al. 2009; Rossi and Menozzi 2012; Rossi et al. 2013). Males grow more rapidly than females and

https://doi.org/10.1017/pab.2016.57 Published online by Cambridge University Press

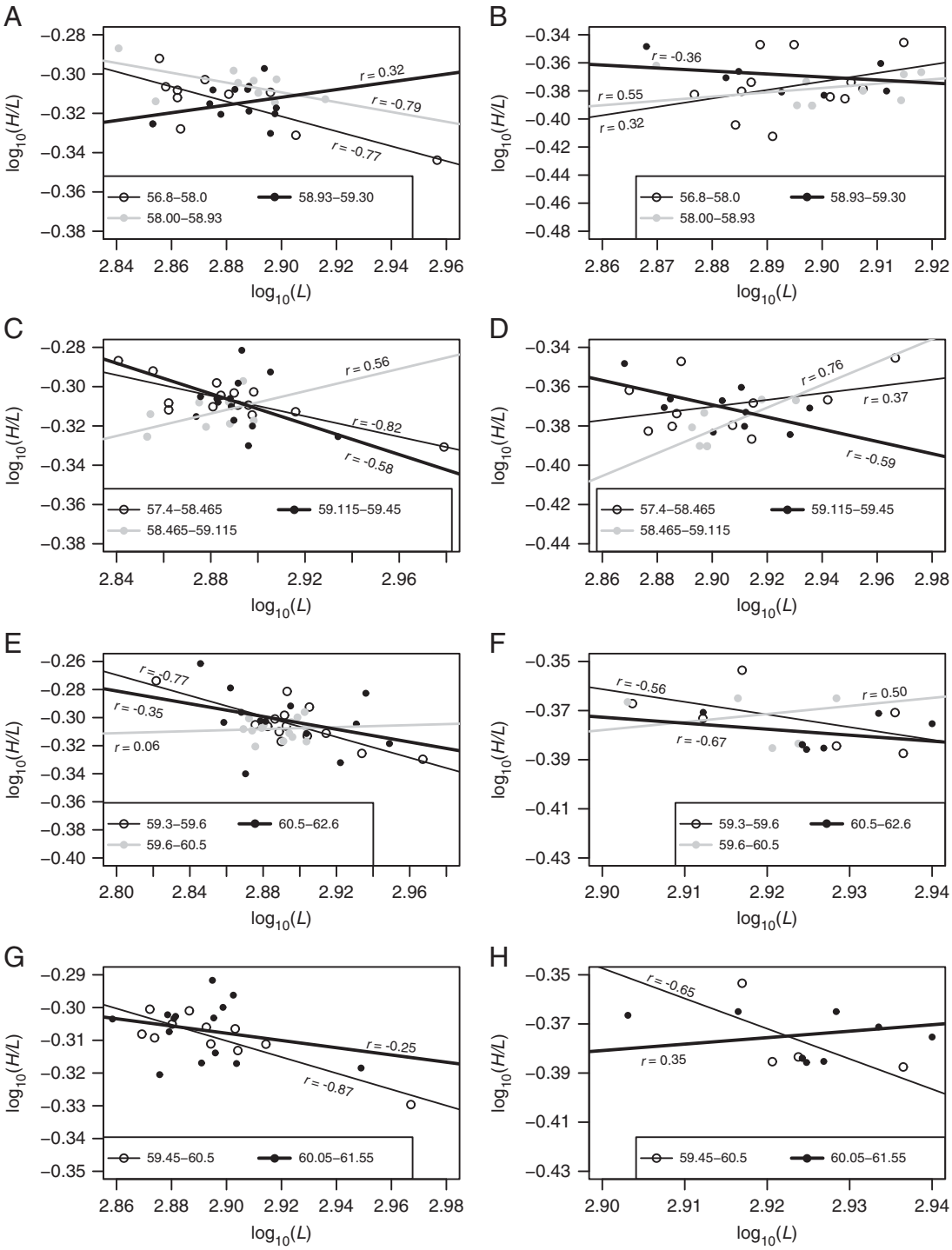

FIGURE 7. Plots of the mean of the H/L ratio versus L in: females (A) and males (B) in the time intervals of 58.0–56.8 Ma, 58.93–58.00 Ma, and 59.30–58.93 Ma; in females (C) and males (D) in the time intervals of 58.465–57.4 Ma, 59.115–58.465 Ma, and 59.450–59.115 Ma; in females (E) and males (F) in the time intervals of 59.6–59.3 Ma, 60.5–59.6 Ma, and 62.6–60.5 Ma; and in females (G) and males (H) in the time intervals of 60.50–59.45 and 61.55–60.05 Ma. In the plotted marks, B is the same as A, D is the same as C, F is the same as E, and H is the same as G. Lines were generated using a simple linear regression model. r is the correlation coefficient. Detailed statistical results are shown in Table 4.

https://doi.org/10.1017/pab.2016.57 Published online by Cambridge University Press

TABLE 4. Result of linear regression analyses between H/L ratios and L in both sexes at each time interval. df, degrees of freedom; R2, coefficient of determination; * significance at 0.05 level; ** significance at 0.01 level.

Time interval (Ma)	Female t	df	p-value	R^2	Male t	df	p-value	R^2
58.000–56.800	−3.4387	8	8.8×10^{-3}**	0.59	1.0849	10	3.0×10^{-1}	0.10
58.465–57.400	−4.9117	12	3.6×10^{-4}**	0.67	1.1103	8	3.0×10^{-1}	0.14
58.930–58.000	−3.6796	8	6.2×10^{-3}**	0.62	1.9591	9	8.0×10^{-2}	0.30
59.115–58.465	1.7654	7	1.2×10^{-1}	0.31	2.5834	5	4.9×10^{-2}*	0.58
59.300–58.930	1.1031	11	2.9×10^{-1}	0.10	−0.93153	6	3.9×10^{-1}	0.13
59.450–59.115	−2.4925	12	2.8×10^{-2}*	0.34	−2.0692	8	7.2×10^{-2}	0.35
59.600–59.300	−4.196	12	1.2×10^{-3}**	0.59	−1.3473	4	2.5×10^{-1}	0.31
60.050–59.450	−5.257	9	5.2×10^{-4}**	0.76	−1.2121	2	3.4×10^{-1}	0.42
60.500–59.600	0.22685	13	8.2×10^{-1}	0.0040	1.1474	4	3.2×10^{-1}	0.25
61.550–60.050	−0.91126	12	3.8×10^{-1}	0.063	1.0423	8	3.3×10^{-1}	0.12
62.600–60.500	−1.2586	11	2.3×10^{-1}	0.12	−2.1867	6	7.1×10^{-2}	0.45

die after copulation (Rossi et al. 2013). In fossil specimens, differences in the maturation rate between the sexes cannot be observed; therefore, the effect of differences in maturation rates can be ruled out. Székely et al. (2014) believe that ASRs are variable between local communities but homogenous at the metapopulation level. We assume fossil ASRs at the metapopulation level. Consequently, we interpret the ASR as indicating the degree of selection pressure on adult males under the assumption of even secondary sex ratios and no taphonomic bias.

The time-series data of the ASRs indicate changes from female-biased to male-biased populations as well as changes in selection pressure on males on the million-year timescale (Fig. 8A). The fossil population shifted to male-biased during the late Paleocene. Our data indicate a shift in the sex bias of the population on evolutionary timescales, as Fisher (1930) predicted, that is, that sex-biased populations must shift to nonbiased populations on evolutionary timescales. According to his idea, intrasex competition in a population changes the sex ratios and eventually makes the ratios reach an equilibrium of 0.5. Our result does not imply that the cause of the shift was competition. The fossil populations constitute 10^5–10^6 generations. The fossil ASRs do not correspond to the operational sex ratios of Emlen and Oring (1977). Their temporal changes indicate an alternation of male mortality rates in the long term. Therefore, our data partially support Fisher's (1930) speculation that the sex-biased population could change its sex ratios on evolutionary timescales.

Durable Valve Shape for Selection Pressure on Males.—Strict stasis is fitted to the temporal change in the H/L ratios of both sexes (Fig. 8B, Table 5). The ratios do not show real evolutionary changes from 63 to 57 Ma. The H/L ratios do not have a correlation with the ASRs, suggesting that the valve shape is insensitive to selection pressure on males (Fig. 6, Table 3). In both sexes, the ratios do not show a correlation. The female valve shape changed independently from the male valve shape, and the female trait was not under the same type of selection as the male trait. Therefore, we believe that the sexual shape dimorphism was not under sexual selection. Our data do not support Abe's (1990) hypothesis on the evolution of sexual shape dimorphism driven by sexual selection.

Function as a Sexual Display Trait.—Our data suggest that the sexual shape dimorphism did not serve as a sexual display trait. The female allometry equation with a slope of −0.388 to −0.247 indicates an inverse allometry ($b<0$) (Supplementary Table 3). The male allometry has the slope of 0.58, showing a negative allometry ($0<b<1$). The types of allometry disagree with the trend of allometry in sexual display. In general, sexual display traits show a positive allometry ($b>1$) (e.g., Green 1992; Petrie 1992; Bonduriansky and Day 2003; Bonduriansky 2007). As mentioned earlier, the valve shape does not correspond to selection pressure on males. Therefore, we believe that the sexual shape dimorphism did not function as a sexual display.

Stability in Allometric Slope and Intercept.—The temporal change in the slope and intercept of the female allometry equation fits the strict stasis model (Fig. 8C,D, Table 5) and supports

https://doi.org/10.1017/pab.2016.57 Published online by Cambridge University Press

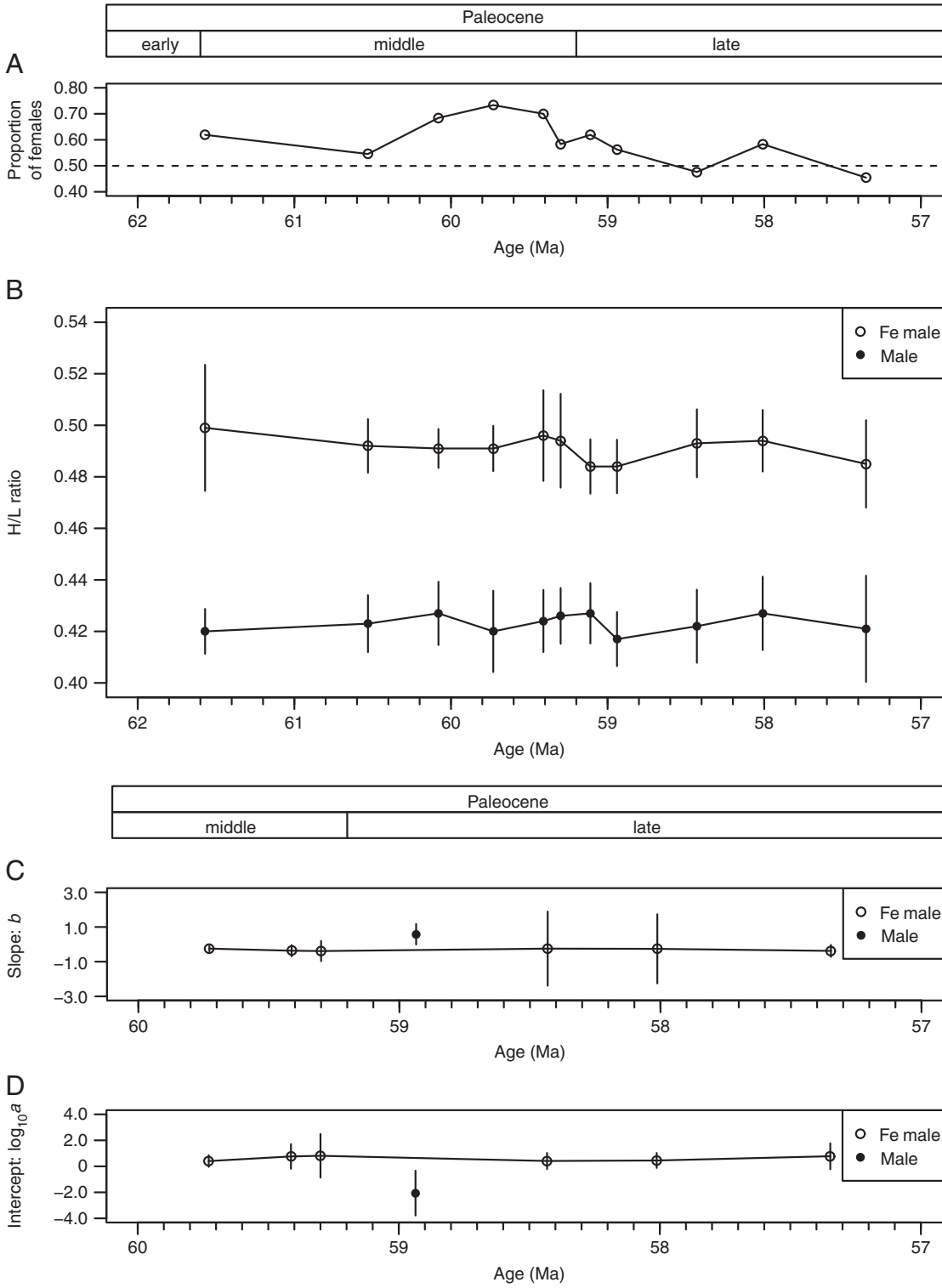

FIGURE 8. Temporal changes in (A) the proportion of females; (B) the mean H/L ratio; (C) b, the allometric slope; and (D) a, the allometric intercept. Vertical bars in B–D indicate ±1 standard deviation.

https://doi.org/10.1017/pab.2016.57 Published online by Cambridge University Press

TABLE 5. Results of the model fits for the time series of mean trait values in both sexes. Directional evolution was modeled as a general random walk. For each model fit, the log-likelihood (lnΛ), number of parameters (*K*), and bias-corrected Akaike information criterion (AICc) are given.

Model		*H/L* ratio						Allometry for female *H/L* ratio					
	K	Female lnΛ	AICc	Akaike weight	Male *lnΛ*	AICc	Akaike weight	Slope lnΛ	AICc	Akaike weight	Intercept lnΛ	AICc	Akaike weight
General random walk	3	44.90	−80.38	9.4×10^{-2}	46.18	−82.93	2.1×10^{-2}	7.1	3.80	0	0.7574	16.49	0
Unbiased random walk	2	43.30	−81.09	1.3×10^{-1}	46.17	−86.83	1.5×10^{-1}	7.1	−6.20	7.0×10^{-2}	0.7523	6.50	7.0×10^{-2}
Stasis	2	43.39	−81.28	1.5×10^{-1}	46.17	−86.83	1.5×10^{-1}	7.1	−6.20	7.0×10^{-2}	0.7523	6.50	7.0×10^{-2}
Strict stasis	1	43.30	−84.15	6.2×10^{-1}	46.17	−89.89	6.8×10^{-1}	7.1	−11.20	8.6×10^{-1}	0.7523	1.50	8.6×10^{-1}
Orstein–Uhlenbeck	4	45.27	−75.86	1.0×10^{-2}	46.28	−77.89	2.0×10^{-3}	7.1	33.79	0	0.7607	46.48	0

the hypothesis of low evaluated allometry slope in the fossil record, as Firmat et al. (2014) reported. Firmat et al. (2014) investigated temporal changes in the allometry of the fossil arvicoline rodent species over the last 600 Kyr. Conversely, Voje et al. (2014) analyzed more than 300 data sets of allometric relationships of animal morphology, which are generally considered to be spread over several millions of years. Voje et al. (2014) predicted stability in the slope on million-year timescales, and the fossil ostracode data have demonstrated this. This stable slope indicates that the evolution of the Paleocene ostracode valve shape is constrained by static allometry.

Conclusions

1. The sexual shape dimorphism in *Krithe dolichodeira* was durable during the Paleocene. It showed no real evolution, even though the selection pressure on males indicates changes. Our study does not support Abe's (1990) hypothesis that a selection pressure on the sexes would drive the evolution of sexual shape dimorphism.
2. The shape dimorphism was not functional for sexual display. It was not correlated with selection pressure on males. The allometry between the shape parameter and the valve length indicate inverse and negative allometry, in contrast to the positive allometry of sexual display traits.
3. The temporal change in the ASRs indicates a shift from a female-biased to a male-biased population on a million-year timescale. Our observation demonstrates Fisher's (1930) speculation that a skewed sex ratio in a population can change on evolutionary timescales.
4. As in Firmat et al. (2014), our result also indicates a stable allometric slope and intercept on million-year timescales. This stable slope suggests that the evolution of the Paleocene valve shape was constrained by static allometry.

Acknowledgments

This research used samples provided by the Integrated Ocean Drilling Program.

https://doi.org/10.1017/pab.2016.57 Published online by Cambridge University Press

We would like to express appreciation to Motomi Genkai-Kato and Gyo Itani (Kochi University) for their constructive advice and discussions on ecology; to Gene Hunt (Smithsonian Institution National Museum of Natural History) and an anonymous reviewer for their review of the manuscript, critical comments, and constructive suggestions; and to Catherine Badgley (University of Michigan) for her editing of the manuscript. This study was financially supported by the Integrated Ocean Drilling Program Expedition 342 After Cruise Research Program of the Japan Agency for Marine–Earth Science and Technology to T.Y., H.M., and H.N. and a scientific fund of the Fujiwara Natural History Public Interest Incorporated Foundation, Japan to T.Y. In addition, we would like to thank Enago (www.enago.jp) for the English-language review.

Literature Cited

Abe, K. 1983. Population structure of *Keijella bisanensis* (Okubo) (Ostracoda, Crustacea)—an inquiry into how far the population structure will be preserved in the fossil record. Journal of the Faculty of Science, the University of Tokyo, Section II 20: 443–488.

——. 1990. What the sex ratios tells us: a case from marine ostracods. Pp. 175–185 *in* R. Whatley, and C. Maybury, eds. Ostracoda and global events. Chapman and Hall, London.

Anderson, D. R., K. P. Burnham, and W. L. Thompson. 2000. Null hypothesis testing: problems, prevalence, and an alternative. Journal of Wildlife Management 64:912–923.

Athersuch, J., D. J. Horne, and J. E. Whittaker. 1989. Marine and brackish water ostracods (superfamilies Cypridacea and Cytheracea): key and notes for the identification of the species. Linnean Society of London and the Estuarine and Brackish-water Sciences Association, Avon, U.K. 343 p.

Ayress, M., T. Barrows, V. Passlow, and R. Whatley. 1999. Neogene to Recent species of *Krithe* (Crustacea: Ostracoda) from the Tasman Sea and off Southern Australia with description of five new species. Records of the Australian Museum 51:1–22.

Badyaev, A. V., and T. E. Martin. 2000. Sexual dimorphism in relation to current selection in the house finch. Evolution 54:987–997.

Badyaev, A. V., L. A. Whittingham, and G. E. Hill. 2001. The evolution of sexual size dimorphism in the house finch. III. Developmental basis. Evolution 55:176–189.

Baltanás, A., M. Otero, L. Arqueros, G. Rossetti, and V. Rossi. 2000. Ontogenetic changes in the carapace shape of the non-marine ostracod *Eucypris virens* (Jurine). Hydrobiologia 148:65–72.

Bonduriansky, R. 2007. Sexual selection and allometry: a critical reappraisal of the evidence and ideas. Evolution 61:838–849.

Bonduriansky, R., and T. Day. 2003. The evolution of static allometry in sexually selected traits. Evolution 57:2450–2458.

Celeux, G., and G. Govaert. 1995. Gaussian parsimonious clustering models. Pattern Recognition 28:781–793.

Cohen, A. C., and J. G. Morin. 1990. Patterns of reproduction in ostracodes: a review. Journal of Crustacean Biology 10:184–211.

Coles, G. P., R. C. Whatley, and A. Moguilevsky. 1994. The ostracod genus *Krithe* from the Tertiary and Quaternary of the North Atlantic. Palaeontology 37:71–120.

Danielopol, D. L., A. Baltanás, T. Namiotko, W. Geiger, M. Pichler, M. Reina, and G. Roidmayr. 2008. Developmental trajectories in geographically separated populations of non-marine ostracods: morphometric applications for palaeoecological studies. Senckenbergiana lethaea 88:183–193.

Dempster, A. P., N. M. Laird, and D. B. Rubin. 1977. Maximum likelihood from incomplete data via the EM algorithm. Journal of the Royal Statistical Society B 39:1–38.

Egset, C. K., T. F. Hansen, A. Le Rouzic, G. H. Bolstad, G. Rosenqvist, and C. Pélabon. 2012. Artificial selection on allometry: change in elevation but not slope. Journal of Evolutionary Biology 25: 938–948.

Emlen, S. T., and L. W. Oring. 1977. Ecology, sexual selection, and the evolution of mating systems. Science 197:215–223.

Fisher, R. A. 1930. The genetical therory of natural selection. Clarendon Press, Oxford. 308. p.

Firmat, C., I. Lozano-Fernández, J. Agustí, G. Bolstad, G. Cuenca-Bescós, T. Hansen, and C. Pélabon. 2014. Walk the line: 600 000 years of molar evolution constrained by allometry in the fossil rodent *Mimomys savini*. Philosophical Transactions of the Royal Society B 369:20140057.

Forel, M.-B., S. Crasquin, A. Chitnarin, L. Angiolini, and M. Gaetani. 2015. Precocious sexual dimorphism and the Lilliput effect in Neo-Tethyan Ostracoda (Crustacea) through the Permian–Triassic boundary. Palaeontology 58:409–454.

Fraley, C., A. E. Raftery, T. B. Murphy, and L. Scrucca. 2012. mclust version 4 for R: normal mixture modeling for model-based clustering, classification, and density estimation (Technical Report No. 597. Department of Statistics, University of Washington, Seattle.

Green, A. J. 1992. Positive allometry is likely with mate choice, competitive display and other functions. Animal Behaviour 43:170–172.

Gradstein, F. M., J. G. Ogg, M. D. Schmitz, and G. M. Ogg. 2012. The Geological Time Scale 2012. Elsevier, Boston.

Hammer, Ø., D. A. T. Harper, and P. D. Ryan. 2001. PAST: paleontological statistics software package for education and data analysis. Palaeontologia Electronica 4:1–9.

Hand, D., H. Mannila, and S. P. 2001. Principles of data mining. MIT Press, Cambridge, Mass. 578. p.

Hansen, T. F. 2012. Adaptive landscapes and macroevolutionary dynamics. Pp. 205–226 *in* E. I. Svensson and R. Clasbeek, eds. The adaptive landscape in evolutionary biology. Oxford University Press, Oxford.

Horne, D. J., A. Cohen, and K. Martens. 2002. Taxonomy, morphology and biology of Quaternary and living Ostracoda. Pp. 5–36. *in* J. A. Holmes, and Allan R. Chivas, eds. The Ostracoda: applications in Quaternary research. American Geophysical Union, Washington, D.C.

Hunt, G. 2004a. Phenotypic variance in fossil samples: modeling the consequences of time-averaging. Paleobiology 30:426–443.

——. 2004b. Phenotypic variance inflation in fossil samples: an empirical assessment. Paleobiology 30:487–506.

——. 2006. Fitting and comparing models of phyletic evolution: random walks and beyond. Paleobiology 32:578–601.

——. 2007a. Evolutionary divergence in directions of high phenotypic variance in the ostracode genus *Poseidonamicus*. Evolution 61: 1560–1576.

——. 2007b. The relative importance of directional change, random walks, and stasis in the evolution of fossil lineages. Proceedings of the National Academy of Sciences USA 104:18404–18408.

——. 2008. Evolutionary patterns within fossil lineages: model-based assessment of modes, rates, punctuations and process. *In* P. H. Kelly, and R. K. Bambach, eds. From evolution to geobiology: research

questions driving paleontology at the start of a new century, Paleontological Society Papers 14: 117–131. Yale University Printing and Publishing Services, New Heaven, Conn.
——. 2013. Testing the link between phenotypic evolution and speciation: an integrated palaeontological and phylogenetic analysis. Methods in Ecology and Evolution 4:714–723.
——. 2015. paleoTS: analyze paleontological time-series. https://CRAN.R-project.org/package=paleoTS.
Hunt, G., and R. E. Chapman. 2001. Evaluating hypotheses of instar-grouping in arthropods: a maximum likelihood approach. Paleobiology 27:466–484.
Hunt, G., and D. L. Rabosky. 2014. Phenotypic evolution in fossil species: pattern and process. Annual Review of Earth and Planetary Sciences 42:421–441.
Hunt, G., and K. Roy. 2006. Climate change, body size evolution, and Cope's Rule in deep-sea ostracodes. Proceedings of the National Academy of Sciences USA 103:1347–1352.
Hunt, G., M. A. Bell, and M. P. Travis. 2008. Evolution toward a new adaptive optimum: phenotypic evolution in a fossil stickleback lineage. Evolution 62:700–710.
Hunt, G., S. A. Wicaksono, J. E. Brown, and K. G. MacLeod. 2010. Climate-driven body-size trends in the ostracode fauna of the deep Indian Ocean. Palaeontology 53:1255–1268.
Hunt, G., M. J. Hopkins, and S. Lidgard. 2015. Simple versus complex models of trait evolution and stasis as a response to environmental change. Proceedings of the National Academy of Sciences USA 112:4885–4890.
Ikeya, N., and H. Ueda. 1988. Morphological variations of *Cytheromorpha acupunctata* (Brady) in continuous populations at Hamana-ko Bay, Japan. Pp. 319–340 *in* T. Hanai, N. Ikeya, and K. Ishizaki, eds. Evolutionary biology of Ostracoda. Elsevier, Amsterdam/Kodansha, Tokyo.
Kamiya, T. 1988. Different sex-ratios in two Recent species of *Loxoconcha* (Ostracoda). Senckenbergiana lethaea 68:337–345.
Knell, R. J., D. Naish, J. L. Tomkins, and D. W. E. Hone. 2013. Sexual selection in prehistoric animals: detection and implications. Trends in Ecology and Evolution 28:38–47.
Lande, R. 1980. Sexual dimorphism, sexual selection, and adaptation in polygenic characters. Evolution 34:292–305.
Martins, M. J. F., J. Vandekerkhove, F. Mezquita, O. Schmit, J. Rueda, T. Namiotko, and G. Rossetti. 2009. Dynamics of sexual and parthenogenetic populations of *Eucypris virens* (Crustacea: Ostracoda) in three temporary ponds. Hydrobiologia 636:219–232.
Matzke-Karasz, R., R. J. Smith, R. Symonova, C. G. Miller, and P. Tafforeau. 2009. Sexual intercourse involving giant sperm in Cretaceous ostracode. Science 324:1535.
Motani, R., D. Jiang, O. Rieppel, Y. Xue, and A. Tintori. 2015. Adult sex ratio, sexual dimorphism and sexual selection in a Mesozoic reptile. Proceedings of the Royal Society B 282:20151658.
Norris, R. D., P. A. Wilson, and P. Blum, and the Expedition 342 Scientists. 2014. Paleogene Newfoundland sediment drifts and MDHDS test. Proceedings of the Integrated Ocean Drilling Program, 342.
Ozawa, H. 2013. The history of sexual dimorphism in Ostracoda (Arthropoda, Crustacea) since the Palaeozoic. Pp. 51–80 *in* H. Moriyama, ed. Sexual dimorphism. InTech, Rijeka, Croatia.
Padian, K., and J. R. Horner. 2013. Misconceptions of sexual selection and species recognition: a response to Knell et al. and to Mendelson and Shaw. Trends in Ecology and Evolution 28:249–250.
Pélabon, C., C. Firmat, G. H. Bolstad, K. L. Voje, D. Houle, J. Cassara, A. Le Rouzic, and T. F. Hansen. 2014. Evolution of morphological allometry. Annals of the New York Academy of Sciences 1320:58–75.
Petrie, M. 1992. Are all secondary sexual display structures positively allometric and, if so, why? Animal Behaviour 43:173–175.
R Core Team. 2015. R: a language and environment for statistical computing.
Reyment, R. A. 1963. Studies on Nigerian Upper Cretaceous and Lower Tertiary Ostracoda. Part 2: Danian, Paleocene, and Eocene Ostracoda. Stockholm Contributions in Geology 10:1–287.
——. 1985. Phenotypic evolution in a lineage of the Eocene ostracod *Echinocythereis*. Paleobiology 11:174–194.
Rossi, V., and P. Menozzi. 2012. Inbreeding and outbreeding depression in geographical parthenogens *Heterocypris incongruens* and *Eucypris virens* (Crustacea: Ostracoda). Italian Journal of Zoology 79:559–567.
Rossi, V., M. Bartoli, C. Bellavere, A. Gandolfi, E. Salvador, and P. Menozzi. 2004. *Heterocypris* (Crustacea: Ostracoda) from the Isole Pelagie (Sicily, Italy): Hatching phenology of resting eggs. Italian Journal of Zoology 71:223–231.
Rossi, V., A. Martorella, and P. Menozzi. 2013. Hatching phenology and voltinism of *Heterocypris barbara* (Crustacea: Ostracoda) from Lampedusa (Sicily, Italy). Journal of Limnology 72:227–237.
Saito-Kato, M., Y. Tanimura, S. Mori, and M. Julius. 2015. Morphological evolution of *Stephanodiscus* (Bacillariophyta) in Lake Biwa from a 300 ka fossil record. Journal of Micropalaeontology 34:165–179.
Schwarz, G. 1978. Estimating the dimension of a model. Annals of Statistics 6:461–464.
Siveter, D. J., G. Tanaka, U. C. Farrell, M. J. Martin, D. J. Siveter, and D. E. G. Briggs. 2014. Exceptionally preserved 450-million-year-old Ordovician ostracods with brood care. Current Biology 24:801–806.
Sheets, H. D., and C. E. Mitchell. 2001. Uncorrected change produces the apparent dependence of evolutionary rate on interval. Paleobiology 27:207–210.
Siepielski, A. M., J. D. DiBattista, and S. M. Carlson. 2009. It's about time: the temporal dynamics of phenotypic selection in the wild. Ecology Letters 12:1261–1276.
Székely, T., A. Liker, R. P. Freckleton, C. Fichtel, and P. M. Kappeler. 2014. Sex-biased survival predicts adult sex ratio variation in wild birds. Proceedings of the Royal Society B 281:20140342.
Tanaka, G. 2016. Redescription of two krithid species (Crustacea, Ostracoda) from the Sea of Japan, with a comment on the taxonomic characters of Krithidae. Paleontological Research 20:31–47.
Vandekerkhove, J., R. Matzke-Karasz, F. Mezquita, and G. Rossetti. 2007. Experimental assessment of the fecundity of *Eucypris virens* (Ostracoda, Crustacea) under natural sex ratios. Freshwater Biology 52:1058–1064.
Voje, K. L., T. F. Hansen, C. K. Egset, G. H. Bolstad, and C. Pélabon. 2014. Allometric constraints and the evolution of allometry. Evolution 68:866–885.
Yamaguchi, T., R. D. Norris, and A. Bornemann. 2012. Dwarfing of ostracodes during the Paleocene–Eocene Thermal Maximum at DSDP Site 401 (Bay of Biscay, North Atlantic) and its implication for changes in organic carbon cycle in deep-sea benthic ecosystem. Palaeogeography, Palaeoclimatology, Palaeoecology 346–347:130–144.
Yamaguchi, T., H. Matsui, and H. Nishi. 2017a. Taxonomy of Maastrichtian–Thanetian deep-sea ostracodes from U1407, IODP Exp 342, off Newfoundland, Northwestern Atlantic. Part 1: Families Cytherellidae, Bairdiidae, Pontocyprididae, Bythocytheridae, and Cytheruridae. Paleontological Research 21:1–22.
——. 2017b. Taxonomy of Maastrichtian–Thanetian deep-sea ostracodes from U1407, IODP Exp 342, off Newfoundland, Northwestern Atlantic, part 2: Families Eucytheridae, Krithidae, Thaerocytheridae, Trachyleberididae, and Xestoleberididae. Paleontological Research 21:97–121.

https://doi.org/10.1017/pab.2016.57 Published online by Cambridge University Press